Autosomal recessive complete STAT1 deficiency caused by compound heterozygous intronic mutations

Sonoko Sakata[1], **Miyuki Tsumura[1], Tadashi Matsubayashi[2], Shuhei Karakawa[1], Shunsuke Kimura[1,12], Moe Tamaura[1], Tsubasa Okano[3], Takuya Naruto[3], Yoko Mizoguchi[1], Reiko Kagawa[1], Shiho Nishimura[1], Kohsuke Imai[3], Tom Le Voyer[4,5], Jean-Laurent Casanova[4–9], Jacinta Bustamante[4,5,8,10], Tomohiro Morio[3], Osamu Ohara[11], Masao Kobayashi[1,13]** and **Satoshi Okada[1]**

[1]Department of Pediatrics, Hiroshima University Graduate School of Biomedical and Health Sciences, Hiroshima 734-8551, Japan
[2]Department of Pediatrics, Seirei Hamamatsu General Hospital, Shizuoka 430-8558, Japan
[3]Department of Pediatrics and Developmental Biology, Graduate School of Medical and Dental Sciences, Tokyo Medical and Dental University, Tokyo 113-8510, Japan
[4]Laboratory of Human Genetics of Infectious Diseases, Necker Branch, INSERM U1163, Necker Hospital for Sick Children, 75015 Paris, France
[5]Paris University, Imagine Institute, 75015 Paris, EU, France
[6]St. Giles Laboratory of Human Genetics of Infectious Diseases, Rockefeller Branch, The Rockefeller University, New York, NY 10065, USA
[7]Pediatric Hematology-Immunology Unit, Necker Hospital for Sick Children, 75015 Paris, EU, France
[8]Study Center of Immunodeficiencies, Necker Hospital for Sick Children, 75015 Paris EU, France
[9]Howard Hughes Medical Institute, New York, NY, USA
[10]Department of Clinical Immunology, Aarhus University Hospital, DK-8200 Aarhus N, EU, Denmark
[11]Department of Applied Genomics, Kazusa DNA Research Institute, Kasarazu 292-0818, Japan
[12]Present address: Department of Pathology, Hematological Malignances Program, St. Jude Children's Research Hospital, Memphis, TN 38105, USA
[13]Present address: Japan Red Cross, Chugoku-Shikoku Block Blood Center, Hiroshima 730-0082, Japan

Correspondence to: S. Okada; E-mail: sokada@hiroshima-u.ac.jp

Abstract

Autosomal recessive (AR) complete signal transducer and activator of transcription 1 (STAT1) deficiency is an extremely rare primary immunodeficiency that causes life-threatening mycobacterial and viral infections. Only seven patients from five unrelated families with this disorder have been so far reported. All causal *STAT1* mutations reported are exonic and homozygous. We studied a patient with susceptibility to mycobacteria and virus infections, resulting in identification of AR complete STAT1 deficiency due to compound heterozygous mutations, both located in introns: c.128+2 T>G and c.542-8 A>G. Both mutations were the first intronic *STAT1* mutations to cause AR complete STAT1 deficiency. Targeted RNA-seq documented the impairment of *STAT1* mRNA expression and contributed to the identification of the intronic mutations. The patient's cells showed a lack of STAT1 expression and phosphorylation, and severe impairment of the cellular response to IFN-γ and IFN-α. The case reflects the importance of accurate clinical diagnosis and precise evaluation, to include intronic mutations, in the comprehensive genomic study when the patient lacks molecular pathogenesis. In conclusion, AR complete STAT1 deficiency can be caused by compound heterozygous and intronic mutations. Targeted RNA-seq-based systemic gene expression assay may help to increase diagnostic yield in inconclusive cases after comprehensive genomic study.

Keywords: mycobacteria, primary immunodeficiency, target RNA sequence, virus

Introduction

Signal transducer and activator of transcription 1 (STAT1) is a latent cytoplasmic transcription factor that has a fundamental role in signal transduction from type I (IFN-α and IFN-β), type II (IFN-γ) and type III (IFN-λ) interferons and also IL-27 (1). In response to IFN-γ, IFN-α/β or IL-27 stimulation, STAT1 forms a homodimer called gamma-interferon activation factor (GAF).

GAF translocates to the nucleus and binds to gamma-activating sequences (GAS) to induce the transcription of target genes involved in antimycobacterial immunity (1, 2). STAT1 also forms a heterotrimer with STAT2, and IRF9, which is known as interferon-stimulated gene factor 3 (ISGF3), after stimulation by IFN-α/β. ISGF3 binds the interferon-stimulated response element (ISRE) and induces target genes involved in anti-viral immunity (1, 2).

Inborn errors in human STAT1 immunity cause at least four types of primary immunodeficiency (PID): (i) autosomal recessive (AR) complete STAT1 deficiency, (ii) AR partial STAT1 deficiency, (iii) autosomal dominant (AD) STAT1 deficiency and (iv) AD STAT1 gain of function (3). Among them, AR complete STAT1 deficiency is an extremely rare PID that causes life-threatening mycobacterial and viral infections. Indeed, only seven patients from five unrelated families with AR complete STAT1 deficiency have been so far reported (3–7). Those patients show complete functional impairment of STAT1-dependent response to type I and type II interferons (4). This is a purely recessive disorder and no haplo-insufficiency at the STAT1 locus has been reported for any of the known cellular or clinical phenotypes (3). Prognosis of the patients with AR complete STAT1 deficiency is poor, and hematopoietic stem cell transplantation (HSCT) is the only curative treatment. Three patients received HSCT and long-term survival was achieved in two patients. Overall, five of the seven patients died before 18 months of age from mycobacterial infections (two patients), viral infections (two patients) or multiorgan failure in the course of HSCT (one patient) (summarized in Table 1) (3, 7). Therefore, early diagnosis and appropriate therapeutic intervention are necessary to avoid life-threatening events in this disorder.

Here, we report a patient with AR complete STAT1 deficiency due to compound heterozygous mutations, c.128+2 T>G/c.542-8 A>G, in *STAT1*. Both mutations were the first intronic *STAT1* mutations reported to cause AR complete STAT1 deficiency. The case reflects the importance of inclusion of non-coding regions and intronic mutations to obtain an accurate clinical diagnosis and precise evaluation in the comprehensive genomic study when the patient lacks molecular pathogenesis. In addition, targeted RNA sequencing (RNA-seq)-based systemic gene expression assay may enhance diagnostic yield in inconclusive cases after comprehensive genomic study.

Methods

Case report

The patient is a 6-year-old Japanese boy who was born to non-consanguineous parents (Fig. 1A). He had no family history of PID. At the age of 1 month, the patient developed respiratory syncytial virus (RSV) bronchiolitis and was treated with non-invasive positive pressure ventilation. He received a Bacillus Calmette–Guérin (BCG) vaccination at 9 months. Five weeks later, the patient developed lymphadenitis in the left axillary region. He then presented with a skin rash and fever. Lymph node biopsy was performed at 11 months. The histopathological finding of the lymph nodes showed no granuloma. *Mycobacterium tuberculosis* was detected by PCR from the lymph nodes and bone marrow. The patient

was started treatment with isoniazid (INH), rifampicin (RFP) and ethambutol (EMB) with the suspicion of *M. tuberculosis* infection. Twenty days later, the vaccine strain BCG was confirmed as the pathogen by southern blotting. Therefore, the patient was given a diagnosis of disseminated BCG. Laboratory tests showed leukocytosis (47 800 μl⁻¹) [reference range (RR) 6000–17 500] and high levels of C-reactive protein (CRP: 10.8 mg dl⁻¹). Serum immunoglobulin levels were normal. The patient displayed normal respiratory burst and normal T-lymphocyte activation after phytohemagglutinin (PHA) or concanavalin A (ConA) stimulation. No obvious abnormality was observed in the T- and B-cell counts, with normal results for T-cell receptor excision circles (TRECs) and K-deleting recombination excision circles (KRECs). Deep and comprehensive phenotyping of immune cell subsets detected a decreased frequency of Th1 cells and myeloid dendritic cells (mDCs), and an increased frequency of Th17 cells (Supplementary Table 1). Since initial antimycobacterial agents were clinically effective, the treatments with INH, RFP and EMB were continued after diagnosis of disseminated BCG. Cumulatively, the patient received INH, RFP and EMB for 40, 28 and 2 months from this episode, respectively. The patient was diagnosed with Mendelian susceptibility to mycobacterial disease (MSMD) and subjected to trio-exome analysis at the age of 11 months. However, trio-exome analysis failed to confirm the genetic etiology at that time.

After that episode, he developed severe and recurrent infections, summarized in Supplementary Table 2. At the age of 1 year and 4 months, he developed acute asthma associated with influenza A infection. The laboratory tests showed an elevated level of serum CRP (12.0 mg dl⁻¹) without the findings of pneumonia on radiological imaging. At the age of 2 years and 1 month, he presented with febrile seizure. The blood examination showed thrombocytopenia (platelets 4.0 × 10⁹ L⁻¹), and elevated levels of serum ferritin (8404 μg L⁻¹, RR 20–250) and soluble IL-2 receptor (8270 U ml⁻¹, RR 157–474). Although no obvious splenomegaly or evidence of hemophagocytosis in the bone marrow was detected, the patient was suspected of having developed hemophagocytic lymphohistiocytosis (HLH) secondary to infection with an unknown pathogen and was successfully treated with dexamethasone palmitate. At the age of 2 years and 11 months, he developed bronchiolitis with a positive result of *Mycoplasma pneumoniae* antigen and treated with azithromycin. At the age of 3 years and 1 month, he developed bilateral tibial osteomyelitis with an elevated level of serum CRP (29.7 mg dl⁻¹). No obvious pathogen was identified from a biopsied specimen by cultivation, and the osteomyelitis did not respond to antibacterial drugs. It gradually improved with a long clinical course. Although there was no evidence, continuous treatment with antimycobacterial agents might have contributed to the improvement of patient's illness. At the age of 3 years and 6 months, he developed pneumonia due to human metapneumovirus (hMPV). He suffered from dyspnea and showed an elevated level of serum CRP (24.5 mg dl⁻¹). At the age of 3 years and 9 months, he developed severe enterocolitis with bilious vomiting and paralytic ileus associated with rotavirus infection. At the age of 3 years and 10 months, he suffered from Kawasaki disease-like symptoms (a combination of fever, rash, swelling of the lips and

Table 1. Summary of the patients with AR complete STAT1 deficiency

Family	Pt	Age at onset (months)	Origin	STAT1 mutations	Mycobacterial infections	Other infections	Outcome	Ref.
1	1	3	Saudi Arabia	c.1757-1758delAG (homozygous)	Disseminated BCG	Recurrent disseminated HSV-1	Died (16 months), disseminated HSV-1 (meningoencephalitis)	(4, 18)
2	2	2	Saudi Arabia	c.1799 T>C (p.L600P) (homozygous)	Disseminated BCG	Severe virus infection (suspected)	Died (12 months), viral-like illness	(4)
2	3	3	Saudi Arabia	c.1799 T>C (p.L600P) (homozygous)	Disseminated mycobacterial disease		Died (3 months)	(3)
2	4	3	Saudi Arabia	c.1799 T>C (p.L600P) (homozygous)	Disseminated mycobacterial disease		Died (3 months)	(3)
3	5	3	Pakistan	c.1928 insA (homozygous)	Disseminated BCG	Polio III, parainfluenza II, rhinovirus, EBV	HSCT (8 months), died (11 months) by fulminant EBV and multiorgan failure	(5)
4	6	10	Pakistan	c.372 G>C p.Q124H (homozygous)	Disseminated *Mycobacterium kansasii*	CMV, HSV-1, sepsis, enterovirus meningitis	HSCT (4 years 7 months), alive with multiple and severe complications	(6, 23)
5	7	8	Australia	c.88delA (homozygous)	No	Multisystem hyper-inflammation, MMR vaccine: encephalopathic, HHV6, HLH	HSCT (14 months), alive	(7)
6	This case	11	Japan	c.128+2 T>G/ c.542-8 A>G (compound heterozygous)	Disseminated BCG *M. malmoense*-positive mediastinal lymphadenitis	RSV, Influenza A, hMPV infections; paralytic ileus by rotavirus; vaccine-induced varicella, HLH	Alive (6 years)	

BCG, Bacillus Calmette–Guérin; CMV, cytomegalovirus; EBV, Epstein–Barr virus; HHV6, human herpesvirus 6; HLH, hemophagocytic lymphohistiocytosis; hMPV, human metapneumovirus; HSCT, hematopoietic stem cell transplantation; HSV, herpes simplex virus; RSV, respiratory syncytial virus.

neck lymph nodes, and conjunctival injection) with elevated atypical lymphocytes and serum CRP (10.2 mg dl^{-1}). These symptoms improved spontaneously without intravenous immunoglobulin treatment. At the age of 4 years and 2 months, he presented with pneumonia, which responded to antibacterial treatment. The prophylaxis with INH was suspended at the age of 4 years and 4 months. At the age of 4 years and 8 months, 2 weeks after receiving his varicella vaccination, he developed vaccine-strain-induced varicella with a typical rash and fever, that was treated with oral acyclovir. At the age of 4 years and 9 months, he developed life-threatening *M. malmoense* mediastinal lymphadenitis and tibial osteomyelitis (Fig. 1B). The histopathological findings of mediastinal lymph node biopsy showed no granuloma formation (Fig. 1C). The symptoms gradually improved after starting RFP, EMB, and clarithromycin (CAM). At the age of 5 years and 4 months, he developed influenza A respiratory infection, which was treated with peramivir (CRP 19.3 mg dl^{-1}).

The systemic gene expression assay with targeted RNA-seq was performed and identified decreased *STAT1* expression with aberrant splicing. The exome data were then reanalyzed, resulting in identification of compound heterozygous intronic mutations, c.128+2 T>G/c.542-8 A>G, in *STAT1*. The patient was thus given a diagnosis of AR complete STAT1 deficiency.

Genomic DNA and whole exome sequencing

Genomic DNA was eluted from whole blood with a QIAamp DNA Mini Kit (Qiagen, Hilden, Germany). Whole exome sequencing (WES) library preparation was performed with SureSelect XT or QXT Reagent Kit (Agilent Technologies, Santa Clara, CA, USA) and SureSelect XT Human All Exon V5 Kit (Agilent Technologies). The library was sequenced using the HiSeq1500 system (Illumina, San Diego, CA, USA), and the variants were annotated as previously described (8). For the first analysis of exome data, we selected the following variants with a global minor allele frequency (GMAF) >0.05 as candidate variants: variants in the cording sequence excluding synonymous variants, variants located within five base points from exon–intron boundaries or variants reported as probably damaging, possibly damaging, disease_causing_automatic, or disease_causing in dbNSPF (https://sites.google.com/site/jpopgen/dbNSFP), or variants reported in OMIM (https://www.ncbi.nlm.nih.gov/omim) or Clinvar (https://www.ncbi.nlm.nih.gov/clinvar/). As for the second analysis (reanalysis) of the exome data, we filtered the variants as previously described (8).

Targeted RNA-seq and expression analysis

Total RNA was extracted from the peripheral blood mononuclear cells (PBMCs) from the patient and 10 other PID patients without genetic etiology after WES. Libraries for the targeted RNA-seq consisting of 426 immune-related genes, which include PID responsible genes reported from International Union of Immunological Societies in 2017 (IUIS 2017), were prepared using an Agilent SureSelect Strand Specific RNA library construction kit with RNAs prepared by the Trizol method (Ambion). RNAs derived from
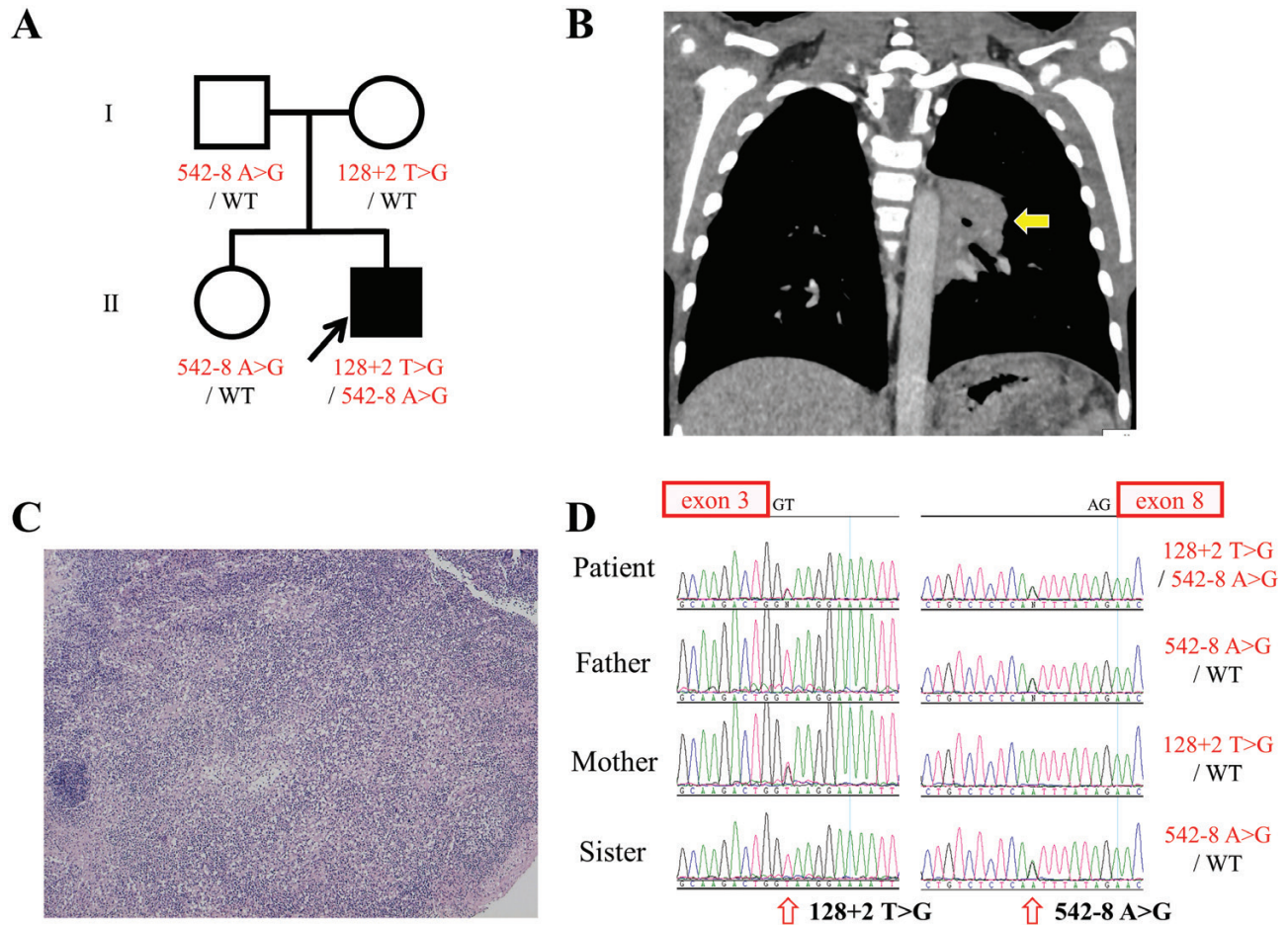
Fig. 1. (A) Family pedigree. The proband is indicated with an arrow. Healthy individuals are shown in white. (B) Chest CT at 4 years 9 months. Mediastinal lymphadenitis is shown with a yellow arrow. (C) Hematoxylin and eosin staining of mediastinal lymph node biopsy shows the infiltration of various inflammatory cells, such as lymphocytes, plasmacytes and neutrophils without granuloma formation. (D) Sanger sequence. Compound heterozygous mutations, c.128+2 T>G and c.542-8 A>G, in STAT1 identified in the patient. His mother carried heterozygous c.128+2 T>G, whereas his father and sister carry the heterozygous c.542-8 A>G mutation.

PID genes were enriched by hybridization with PID panel probes using a SureSelect target enrichment system (Agilent Technologies). The enriched libraries were sequenced on an Illumina MiSeq under a 75-base paired-end run mode and the obtained reads were mapped to the human reference genome (NCBI build 37.1) using STAR (9, 10). For expression analysis, the count data were extracted using Rsubread (11) and normalized using DESeq2 (12). To analyze the effect of splice-site mutations, the splicing pattern was assessed manually with IGV software (13).

The detailed methods of quantitative PCR and reverse transcription PCR (RT-PCR) are shown in the Supplementary Methods.

Flow cytometry

The PBMCs were isolated by density gradient centrifugation. The PBMCs were suspended at a density of 10^4 cells μl^{-1} in serum-free RPMI1640. The cells were incubated with IFN-γ (1000 IU ml^{-1}) or IFN-α (1000 IU ml^{-1}) for 15 min at 37°C in the presence of FITC-conjugated CD14 (BD Biosciences, Franklin Lakes, NJ, USA). They were then washed in

RPMI1640 and were fixed and permeabilized according to the BD Phosflow protocol (Protocol III). They were next stained with FITC-conjugated anti-CD14 and PE-conjugated anti-pSTAT1 (pY701) (BD Biosciences), and subjected to flow cytometric analysis to analyze STAT1 phosphorylation. Data were analyzed with FlowJo software (BD Biosciences).

Immunoblot analysis and electrophoretic mobility shift assay

The PBMCs or SV40 fibroblasts were incubated in the presence or absence of IFN-γ (1000 IU ml^{-1}) or IFN-α (1000 IU ml^{-1}) for 15 min and subjected to immunoblot analysis. Immunoblot analysis was performed as described previously (14, 15). The following primary antibodies used for immunoblotting: an anti-pSTAT1 (pY701) antibody (Cell Signaling Technology, Danvers, MA, USA), an anti-STAT1α antibody against total STAT1 (Santa Cruz Biotechnology, Santa Cruz, CA, USA) and an anti-β-actin antibody (Sigma-Aldrich, St. Louis, MO, USA). Electrophoretic mobility shift assay (EMSA) was conducted as previously described (15, 16). Briefly, the cells were stimulated by incubation for 15 min with 1000 IU
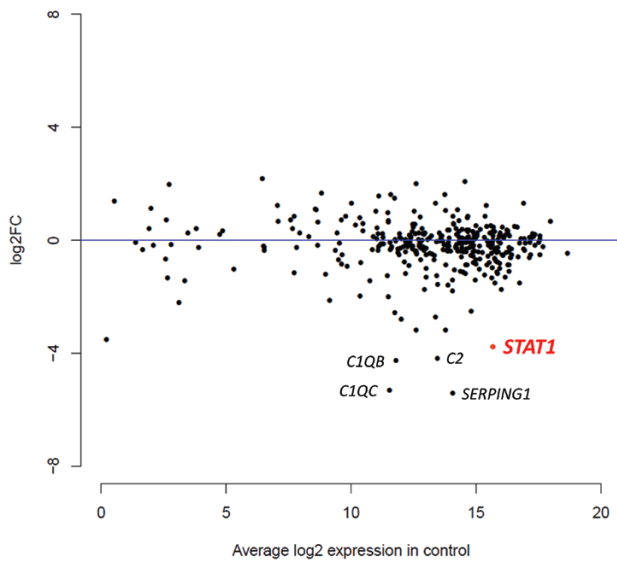
Fig. 2. Dysregulated STAT1 expression in the patient's PBMCs. MAplot showing differentially expressed genes in the patient compared with inconclusive PID patients (control, n = 10) analyzed by target RNAseq. Each plot displays genes in the target RNAseq panel (n = 426). Count data of each gene was obtained by Rsubread and normalized with DESeq2. The X axis indicates average log2 expression of normalized counts in control and the Y axis represents the log2 fold change (Log2FC) of normalized counts in the patient against average normalized counts of control.

ml^{-1} IFN-γ or 1000 IU ml^{-1} IFN-α. We then incubated 10 μg of nuclear extract with ^{32}P-labeled (αdATP) GAS (from *FCGR1* promoter) or ISRE (from *ISG15* promoter) probes for 30 min and subjected them to analysis.

Ethics statement

We obtained written informed consent for genomic analysis and blood sample-based functional studies of the patient, parents and siblings in accordance with the Declaration of Helsinki. The genetic analysis and blood sample based functional studies were approved by the Institutional Review Board of Hiroshima University and Tokyo Medical and Dental University.

Results

Identification of biallelic variants in STAT1

High-molecular-weight genomic DNA was extracted from peripheral blood. Trio-WES, which was performed at 11 months of age, identified a novel heterozygous variant, c.128+2 T>G, in the *STAT1* gene in the patient and his asymptomatic mother (Fig. 1A and D). Rare variants in other known PID-related genes reported in IUIS 2017 (*LRBA*, *NBN*, *NHEJ1* and *TBX1*) were also identified (Supplementary Table 3) (10). However, they were not inferred to be disease-causing based on the clinical manifestations and their inheritance pattern. The c.128+2 T>G *STAT1* variant was confirmed by Sanger sequencing (Fig. 1D). Monoallelic dominant negative and loss-of-function mutations in *STAT1*, which are normally expressed at the protein level, have been identified in

patients with MSMD (2, 15–20). In contrast, a familial study of patients with AR STAT1 complete deficiency, which investigated parents with monoallelic loss-of-expression mutation in *STAT1*, revealed that there is no haploinsufficiency at the *STAT1* locus (3). The c.128+2 T>G variation identified in this study's patient was located at an essential splice site and was suspected to disturb STAT1 protein expression. Based on a previous study that showed a lack of haploinsufficiency, together with the presence of this variant in the asymptomatic mother, the pathogenicity of the c.128+2 T>G variant was missed at the first analysis of the exome data.

A systemic gene expression assay using targeted RNA-seq identified decreased STAT1 expression and exon skipping at exon 8 of *STAT1*. We thus thoroughly reanalyzed the exome data and identified a novel heterozygous intronic variant, c.542-8A>G, which was missed by the filtering process of first analysis of the exome data (filtering strategy of the first analysis of exome data is detailed in Methods). This variant was confirmed by Sanger sequencing and was identified in the asymptomatic father and elder sister (Fig. 1A and D). Therefore, the patient was determined to have compound heterozygous variations, c.128+2 T>G/c.542-8 A>G, in *STAT1*. Neither variant was found in the Single Nucleotide Polymorphism Database (dbSNP), 1000 Genome Projects, the Exome Aggregation Consortium (ExAc) database or the genome aggregation database (gnomAD).

Targeted RNA-seq and qPCR

A targeted RNA-seq-based systemic gene expression assay of PBMCs was implemented to investigate the molecular pathogenesis of the patient. This assay ranked *STAT1* as among the top five genes with reduced expression in the patients when we used the other 10 inconclusive PID patients as controls (Fig. 2). As expected, the splicing pattern assessed manually with IGV software revealed intron retention at exon 3 associated with the c.128+2 T>G variant (Fig. 3A). Furthermore, we identified abnormal splicing in the form of exon skipping at exon 8 of the *STAT1* gene (Fig. 3B). We next performed an RT-PCR assay for STAT1 from PBMCs of the patient and two healthy individuals. The RT-PCR assay, which spanned exon 3 and exon 7 of *STAT1*, confirmed the reduced expression of *STAT1* mRNA and the presence of intron retention by detecting approximate 1350 bp band in the patient (Supplementary Figure S1). The RT-PCR assay, which spanned exon 6 and exon 10 of *STAT1*, also confirmed the presence of exon skipping at exon 8 by detecting approximate 300 bp band in the patient. To confirm the result of the targeted RNA-seq and evaluate the impact of the biallelic *STAT1* variations on mRNA synthesis, we carried out qPCR from PBMCs of the patient and a healthy control. This confirmed a severe decrease of *STAT1* mRNA in the patient's cells (9.4% of *STAT1* mRNA compared with the control's) (Fig. 4A).

Impaired STAT1 protein expression and phosphorylation

We performed flow cytometry to analyze the STAT1 function by detecting its phosphorylation (pSTAT1) upon IFN-γ or IFN-α stimulation. The CD14$^+$ monocytes from a healthy control showed pSTAT1 upon IFN-γ or IFN-α (Fig. 4B). In contrast, the CD14$^+$ monocytes from the patient completely lacked
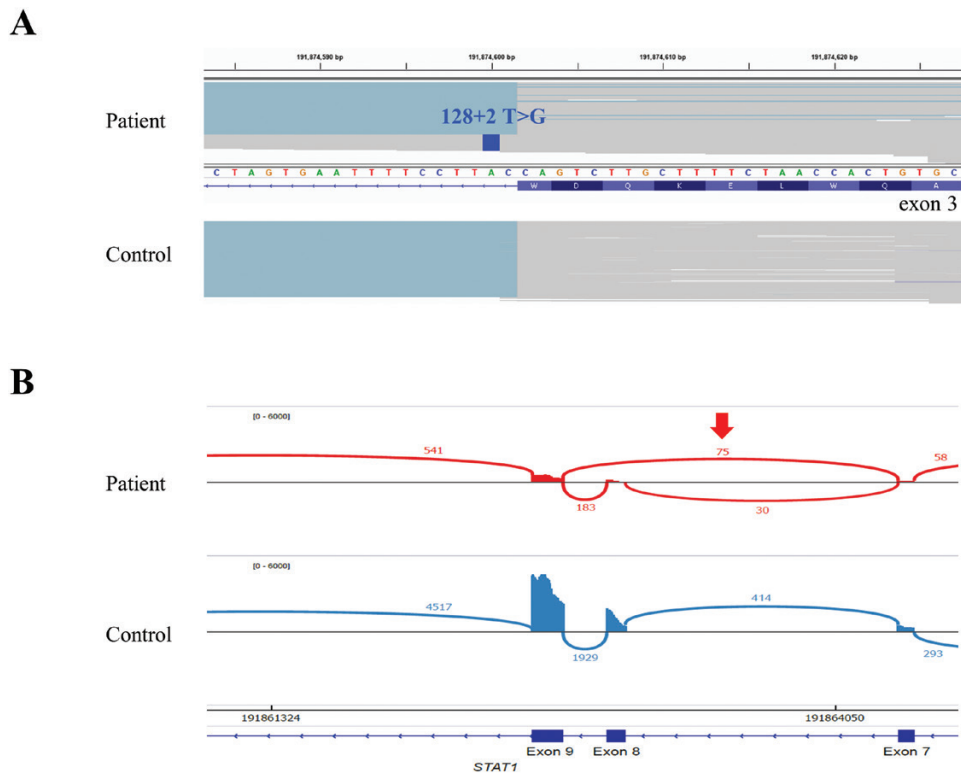
A

B

Fig. 3. Biallelic abnormal splicing of STAT1 in the patient detected by targeted RNAseq. (A) The c.128+2 T>G STAT1 mutation induced intron retention at exon 3, which was shown by IGV software with the coverage over the intronic region (gray lines) only in the patient sample (upper panel). (B) Exon skipping at exon 8 (red arrow) as a result of the c.542-8 A>G mutation was shown with a Sashimi plot. Each line (red line: patient, blue line: normal) and number indicate junctions and read counts, respectively

pSTAT1 in response to IFN-γ or IFN-α. To confirm this finding, PBMCs from the patient and a healthy control were stimulated with IFN-γ or IFN-α and subjected to immunoblot analysis. As shown in Fig. 4C, PBMCs from the patient showed a complete lack of STAT1 protein expression and its phosphorylation upon IFN-γ or IFN-α stimulation. These results are comparable to the patient's clinical manifestations, showing a series of severe mycobacterial and viral infection, together with identifying a lack of granuloma formation associated with mycobacteria infection. Taken together, the biallelic variations identified in the patient were determined to be pathogenic mutations. The patient was thus given a diagnosis of AR complete STAT1 deficiency.

STAT1 phosphorylation and DNA-binding ability in SV40-transformed fibroblasts

To confirm the molecular defects observed in the patient's PBMCs, we assessed the STAT1 protein and phosphorylation using SV40-transformed fibroblasts (SV40 fibroblast) from the patient, two healthy controls and a disease control from a patient with AR complete STAT1 deficiency (STAT1^{−/−}). The SV40 fibroblasts from the patient, as well as STAT1^{−/−} SV40 fibroblasts, showed a complete lack of STAT1 protein expression and its phosphorylation upon IFN-γ and IFN-α stimulation (Fig. 5A). Next, the DNA-binding ability of the wild-type (WT) and mutant STAT1 proteins was analyzed by EMSA. The SV40 fibroblasts were stimulated with IFN-γ or IFN-α for 15 min and

subjected to EMSA. As shown in Fig. 5(B), SV40 fibroblasts from the patient, as well as the STAT1^{−/−} SV40 fibroblasts, presented a complete loss of DNA-binding activity to GAS in response to IFN-γ or IFN-α stimulation. These results suggested that not only PBMCs but also SV40 fibroblasts from the patient lacked a cellular response to IFN-γ or IFN-α.

Impaired cellular response to IFN-γ and IFN-α

STAT1 plays a non-redundant role in the up-regulation of target genes upon IFN-γ and IFN-α stimulation. The CD14^{+} monocytes from the patient and controls were stimulated with IFN-γ (100 IU ml^{−1}) or IFN-α (100 IU ml^{−1}) for 6 h. They were then subjected to RNA-seq. The patient's CD14^{+} monocytes showed global dysregulation of STAT1 target genes upon the monocytes being stimulated with IFN-γ and IFN-α (Fig. 6). These results suggest that the patient's cells display impaired responses to IFN-γ and IFN-α.

Discussion

We herein reported a patient with AR complete STAT1 deficiency due to *STAT1* compound heterozygous mutations, both located in introns: c.128+2 T>G and c.542-8 A>G. Both mutations were private and absent from the public databases. Five mutations in *STAT1* have been reported to cause AR complete STAT1 deficiency in previous studies (3–7). All of the previously reported *STAT1* mutations are located in exonic regions and have been identified in the homozygous state.
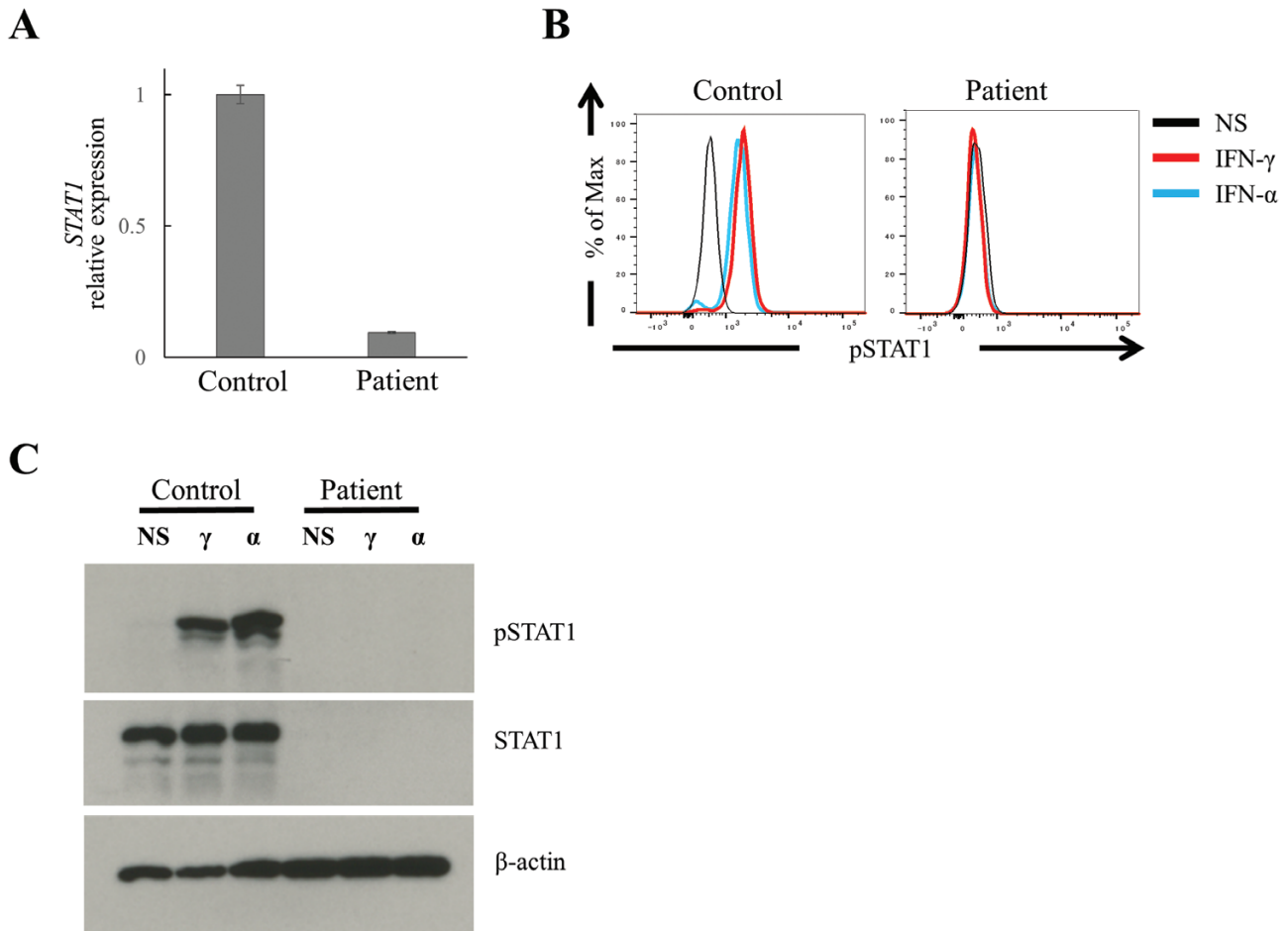
A

B

C

Fig. 4. (A) Expression of STAT1 mRNA in PBMCs from the patient and a healthy control. Target gene expression was normalized against GAPDH and presented as *n*-fold increase over the expression in the healthy control. (B) Flow cytometry analysis of STAT1 phosphorylation in CD14$^+$ cells after stimulation with IFN-γ (1000 IU ml^{-1}, red line) or IFN-α (1000 IU ml^{-1}, blue line). (C) Immunoblot analysis of STAT1 protein and its phosphorylation in PBMCs from the patient and a healthy control. The PBMCs were stimulated with IFN-γ (1000 IU ml^{-1}) or IFN-α (1000 IU ml^{-1}) for 15 min for the analysis. NS: no stimulation; γ: IFN-γ; α: IFN-α

A

B
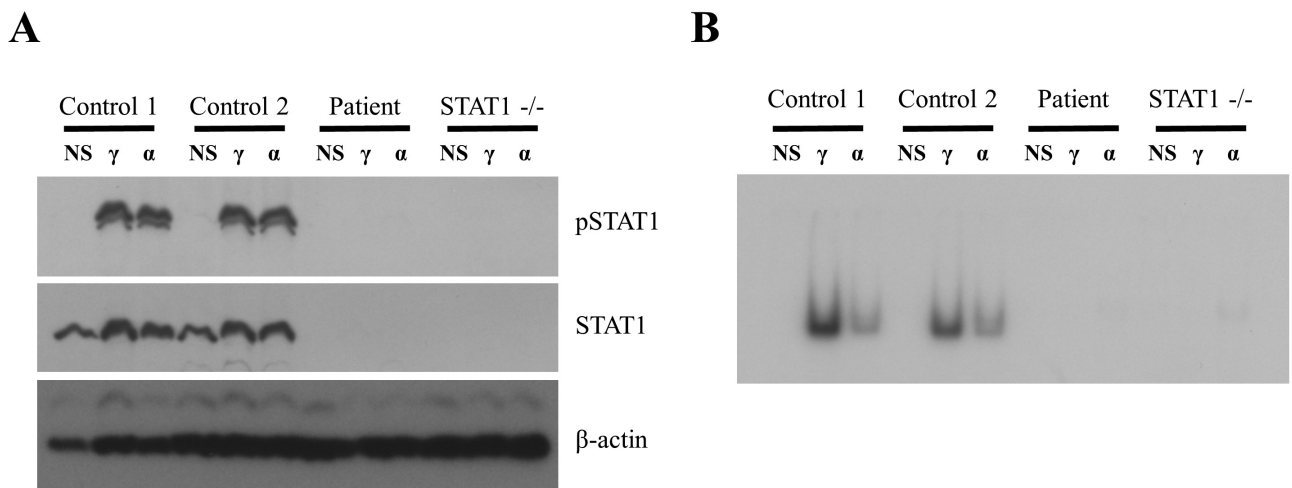
Fig. 5. (A) The SV40 fibroblasts from the patient and STAT1$^{-/-}$ SV40 fibroblasts showed complete lack of STAT1 protein expression and its phosphorylation upon IFN-γ and IFN-α. NS: no stimulation; γ: IFN-γ; α: IFN-α (B) The DNA-binding ability of the WT and mutant STAT1 proteins was analyzed by EMSA. The SV40 fibroblasts from the patient, as well as STAT1$^{-/-}$ SV40 fibroblasts, presented complete loss of DNA-binding activity to GAS in response to IFN-γ or IFN-α. NS: no stimulation; γ: IFN-γ; α: IFN-α.
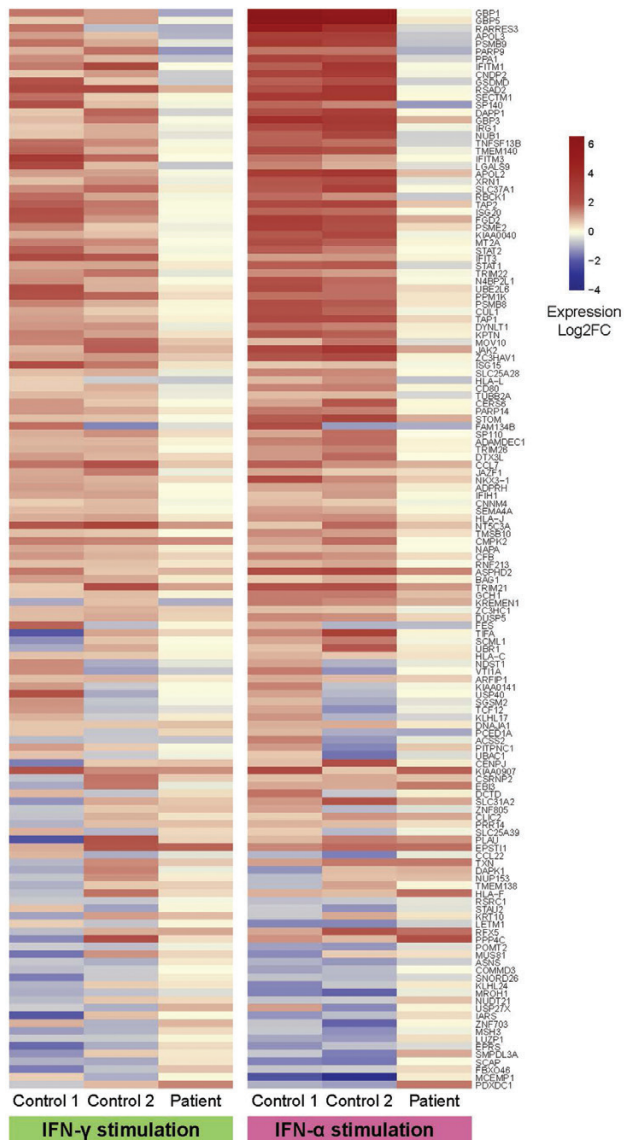
Fig. 6. Global dysregulation of STAT1 target genes upon IFN-γ and IFN-α stimulation in patient's CD14⁺ monocytes. The CD14⁺ monocytes from the patient and controls were stimulated with IFN-γ (100 IU ml⁻¹; left) or IFN-α (100 IU ml⁻¹; right) for 6 h and subjected to RNA sequencing. Log2FC: Log2 fold change.

Therefore, the current case is the first AR complete STAT1 deficiency due to intronic *STAT1* mutations. These mutations resulted in severe impairment of *STAT1* mRNA expression. The c.128+2 T>G mutation was identified by WES during the first data analysis, whereas the c.542-8 A>G mutation was missed at that time because the default filtering strategy stringently excluded intronic variants beyond five base pairs from the exon–intron boundary. Monoallelic loss-of-function *STAT1* mutations, which results in normal expression and exert a dominant negative effect on WT STAT1-mediated IFN-γ signaling, specifically disturb host immunity to mycobacteria and cause MSMD (called AD partial STAT1 deficiency). In contrast, the previous studies, which analyzed relatives of cases with AR complete STAT1 deficiency, clearly show a lack of

haploinsufficiency in human STAT1 (3–7, 21–23). The patient in the present study was clinically diagnosed as MSMD when the first exome data analysis was performed. The pathogenicity of the c.128+2 T>G mutations was thus missed at that time because the mutations were inherited from the patient's asymptomatic mother and predicted to disturb STAT1 protein expression by disturbing its splicing.

The identification of intronic mutations by comprehensive genomic study can be challenging. Such mutations are easily missed in the filtering process of considerable numbers of variants of unknown significance (VUS) in the analysis of exome data. Reflecting this difficulty, it took nearly 4 years to confirm the molecular cause in the current study. To investigate PID-related genes with a low expression level effectively, we performed targeted RNAseq, which enriched 426 immune-related genes, by focusing on PBMCs. This assay successfully ranked STAT1 as one of the top five genes with reduced expression in the patient when we used another 10 inconclusive PID patients as controls. This assay also detected exon skipping at exon 8 of *STAT1* due to the c.542-8 A>G mutation. The results suggested that targeted RNAseq is a potentially useful diagnostic tool for identifying inconclusive PID patients after WES. Recent studies revealed that RNAseq-based comprehensive transcriptomic analysis is a useful tool for detecting mis-splicing, which improved the diagnostic yield of inconclusive cases by WES. This in turn led to an approximately 10–35% increase in the detection of pathogenic variants (24–26). One major difficulty in transcriptomic analysis is tissue-specific expression (26). Regarding this point, PID has an advantage as a target disease for RNA-seq because we can use PBMCs for analysis. However, the introduction of RNA-seq in the diagnosis of PID patients is still in its primitive stage.

After the first genetic study, which was performed at the age of 11 months, the patient presented over the following several years with several episodes of severe virus infections. He developed severe influenza A infection (at 1 and 5 years old), hMPV pneumonia (at 3 years old), enterocolitis and paralytic ileus by rotavirus (at 3 years old) and vaccine-strain induced varicella (at 4 years old). Especially, the episodes of paralytic ileus by rotavirus and vaccine-strain induced varicella strongly suggested that the patient was prone to viruses. Retrospectively, these infectious phenotypes, together with the histopathological finding of mycobacterial lymphadenitis, which lacked granuloma formation, suggested AR complete STAT1 deficiency as a differential diagnosis. Indeed, the lack of granuloma formation is a typical finding in patients with AR complete IFN-γR1, IFN-γR2 or STAT1 deficiency (27, 28). However, the clinical rarity and lack of awareness of AR complete STAT1 deficiency makes suspicion of this disorder unlikely. The delayed diagnosis in the current study highlights the importance of clinical information and recognition of the characteristic findings of specific disorders to minimize overlooking pathogenic mutations in WES. Genetic diagnosis brings significant change in management in 25–37% of patients with PID (29, 30). Indeed, it was decided that the patient in the present study should undergo HSCT after confirming the molecular diagnosis of AR complete STAT1 deficiency. However, the diagnostic yield of next-generation sequencing in PID patients ranges from 15 to 46%

(median = 25%) ([31](#)) and has room for improvement. The experience of the case presented in this study suggests that the introduction of targeted RNAseq has the potential to improve the diagnostic yield of patients with PID.

References

1 Stark, G. R., Kerr, I. M., Williams, B. R., Silverman, R. H. and Schreiber, R. D. 1998. How cells respond to interferons. *Annu. Rev. Biochem.* 67:227.

2 Hirata, O., Okada, S., Tsumura, M. *et al.* 2013. Heterozygosity for the Y701C STAT1 mutation in a multiplex kindred with multifocal osteomyelitis. *Haematologica* 98:1641.

3 Boisson-Dupuis, S., Kong, X. F., Okada, S. *et al.* 2012. Inborn errors of human STAT1: allelic heterogeneity governs the diversity of immunological and infectious phenotypes. *Curr. Opin. Immunol.* 24:364.

4 Dupuis, S., Jouanguy, E., Al-Hajjar, S. *et al.* 2003. Impaired response to interferon-alpha/beta and lethal viral disease in human STAT1 deficiency. *Nat. Genet.* 33:388.

5 Chapgier, A., Wynn, R. F., Jouanguy, E. *et al.* 2006. Human complete Stat-1 deficiency is associated with defective type I and II IFN responses *in vitro* but immunity to some low virulence viruses *in vivo. J. Immunol.* 176:5078.

6 Vairo, D., Tassone, L., Tabellini, G., *et al.* 2011. Severe impairment of IFN-gamma and IFN-alpha responses in cells of a patient with a novel STAT1 splicing mutation. *Blood* 118:1806.

7 Burns, C., Cheung, A., Stark, Z. *et al.* 2016. A novel presentation of homozygous loss-of-function STAT-1 mutation in an infant with hyperinflammation—a case report and review of the literature. *J. Allergy Clin. Immunol. Pract.* 4:777.

8 Naruto, T., Okamoto, N., Masuda, K. *et al.* 2015. Deep intronic GPR143 mutation in a Japanese family with ocular albinism. *Sci. Rep.* 5:11334.

9 Dobin, A., Davis, C. A., Schlesinger, F. *et al.* 2013. STAR: ultrafast universal RNA-seq aligner. *Bioinformatics* 29:15.

10 Picard, C., Bobby Gaspar, H., Al-Herz, W. *et al.* 2018. International Union of Immunological Societies: 2017 Primary Immunodeficiency Diseases Committee Report on Inborn Errors of Immunity. *J. Clin. Immunol.* 38:96.

11 Liao, Y., Smyth, G. K. and Shi, W. 2019. The R package Rsubread is easier, faster, cheaper and better for alignment and quantification of RNA sequencing reads. *Nucleic Acids Res.* 47:e47.

12 Love, M. I., Huber, W. and Anders, S. 2014. Moderated estimation of fold change and dispersion for RNA-seq data with DESeq2. *Genome Biol.* 15:550.

13 Robinson, J. T., Thorvaldsdóttir, H., Winckler, W. *et al.* 2011. Integrative genomics viewer. *Nat. Biotechnol.* 29:24.

14 Mizoguchi, Y., Tsumura, M., Okada, S. *et al.* 2014. Simple diagnosis of STAT1 gain-of-function alleles in patients with chronic mucocutaneous candidiasis. *J. Leukoc. Biol.* 95:667.

15 Kagawa, R., Fujiki, R., Tsumura, M. *et al.* 2017. Alanine-scanning mutagenesis of human signal transducer and activator of transcription 1 to estimate loss- or gain-of-function variants. *J. Allergy Clin. Immunol.* 140:232.

16 Tsumura, M., Okada, S., Sakai, H. *et al.* 2012. Dominant-negative STAT1 SH2 domain mutations in unrelated patients with Mendelian susceptibility to mycobacterial disease. *Hum. Mutat.* 33:1377.

17 Ueki, M., Yamada, M., Ito, K. *et al.* 2017. A heterozygous dominant-negative mutation in the coiled-coil domain of STAT1 is the cause of autosomal-dominant Mendelian susceptibility to mycobacterial diseases. *Clin. Immunol.* 174:24.

18 Dupuis, S., Dargemont, C., Fieschi, C. *et al.* 2001. Impairment of mycobacterial but not viral immunity by a germline human STAT1 mutation. *Science* 293:300.

19 Chapgier, A., Boisson-Dupuis, S., Jouanguy, E. *et al.* 2006. Novel STAT1 alleles in otherwise healthy patients with mycobacterial disease. *PLoS Genet.* 2:e131.

20 Sampaio, E. P., Bax, H. I., Hsu, A. P. *et al.* 2012. A novel STAT1 mutation associated with disseminated mycobacterial disease. *J. Clin. Immunol.* 32:681.

21 Chapgier, A., Kong, X. F., Boisson-Dupuis, S. *et al.* 2009. A partial form of recessive STAT1 deficiency in humans. *J. Clin. Invest.* 119:1502.

22 Kong, X. F., Ciancanelli, M., Al-Hajjar, S. *et al.* 2010. A novel form of human STAT1 deficiency impairing early but not late responses to interferons. *Blood* 116:5895.

23 Naviglio, S., Soncini, E., Vairo, D., Lanfranchi, A., Badolato, R. and Porta, F. 2017. Long-term survival after hematopoietic stem cell transplantation for complete STAT1 deficiency. *J. Clin. Immunol.* 37:701.

24 Landrith, T., Li, B., Cass, A. A. *et al.* 2020. Splicing profile by capture RNA-seq identifies pathogenic germline variants in tumor suppressor genes. *NPJ Precis. Oncol.* 4:4.

25 Deelen, P., van Dam, S., Herkert, J. C. *et al.* 2019. Improving the diagnostic yield of exome- sequencing by predicting gene-phenotype associations using large-scale gene expression analysis. *Nat. Commun.* 10:2837.

26 Marco-Puche, G., Lois, S., Benítez, J. and Trivino, J. C. 2019. RNA-Seq perspectives to improve clinical diagnosis. *Front. Genet.* 10:1152.

27 Bustamante, J., Boisson-Dupuis, S., Abel, L. and Casanova, J. L. 2014. Mendelian susceptibility to mycobacterial disease: genetic, immunological, and clinical features of inborn errors of IFN-γ immunity. *Semin. Immunol.* 26:454.

28 Emile, J. F., Patey, N., Altare, F. *et al.* 1997. Correlation of granuloma structure with clinical outcome defines two types of idiopathic disseminated BCG infection. *J. Pathol.* 181:25.

29 Stray-Pedersen, A., Sorte, H. S., Samarakoon, P. *et al.* 2017. Primary immunodeficiency diseases: genomic approaches delineate heterogeneous Mendelian disorders. *J. Allergy Clin. Immunol.* 139:232.

30 Rae, W., Ward, D., Mattocks, C. *et al.* 2018. Clinical efficacy of a next-generation sequencing gene panel for primary immunodeficiency diagnostics. *Clin. Genet.* 93:647.

31 Yska, H. A. F., Elsink, K., Kuijpers, T. W., Frederix, G. W. J., van Gijn, M. E. and van Montfrans, J. M. 2019. Diagnostic yield of next generation sequencing in genetically undiagnosed patients with primary immunodeficiencies: a systematic review. *J. Clin. Immunol.* 39:577.